

Flow over a cylinder Part I: Numerical analysis with Ansys Fluent

Fluids Mechanics II

Laboratory session 1



14th of March, 2025

Authors:

Diego Delgado Madrigal

Lidia Mena Cardeña

Jon Castillo Altube

Andrés Velázquez Vela

1 Introduction

This session's purpose was to model the flow past a cylinder numerically Ansys Fluent. An analysis for different values of the Reynolds number will be made and the von Kármán vortex street will be reproduced, one for a low Reynolds number, another one for a moderate Reynolds number, another one for a large Reynolds number and, finally, the last one for the Boundary Layer separation, in order to analyze different flow phenomena, such as laminar flow or turbulent wakes.

2 Objectives

The main objectives for this laboratory practice are:

1. Analyze the effect of the Reynolds number on the flow characteristics around a circular cylinder.
2. Observe and reproduce the von Kármán vortices, studying its formation and frequency of oscillation.
3. Simulate and compare different flow conditions using Ansys Fluent, ensuring numerical convergence and reliability of results.
4. Validate numerical results by comparing them with theoretical predictions and previous data.

3 Numerical Methodology

3.1 a) Application of the Π Theorem

To demonstrate that the resulting flow pattern depends solely on the Reynolds number, we begin by applying dimensional analysis using the Buckingham Π theorem.

Let us consider the relevant physical parameters: the diameter of the cylinder d , the upstream velocity U_∞ , the fluid density ρ , and the kinematic viscosity ν . We assume the drag force D is the dependent variable. Their dimensions are:

$$\begin{aligned} d &= [L] \\ U_\infty &= [L][T]^{-1} \\ \rho &= [M][L]^{-3} \\ \nu &= [L]^2[T]^{-1} \\ D &= [M][L][T]^{-2} \end{aligned}$$

We express the functional dependence as:

$$D = f(d, U_\infty, \rho, \nu)$$

According to Buckingham's Π theorem, we construct two dimensionless groups Π_1 and Π_2 .

First Group Π_1

Let:

$$\Pi_1 = D \cdot d^a \cdot U_\infty^b \cdot \rho^c$$

We require:

$$[M^0 L^0 T^0] = [MLT^{-2}] \cdot [L]^a \cdot [LT^{-1}]^b \cdot [ML^{-3}]^c$$

Matching dimensions:

$$\text{Mass (M): } 0 = 1 + c \Rightarrow c = -1$$

$$\text{Length (L): } 0 = 1 + a + b - 3c \Rightarrow a = -2$$

$$\text{Time (T): } 0 = -2 - b \Rightarrow b = -2$$

Therefore:

$$\Pi_1 = \frac{D}{\rho U_\infty^2 d^2}$$

This is the well-known drag coefficient:

$$C_D = f(\Pi_2)$$

Second Group Π_2

Let:

$$\Pi_2 = \nu \cdot d^a \cdot U_\infty^b \cdot \rho^c$$

Again, matching dimensions:

$$[L^0 T^0 M^0] = [L^2 T^{-1}] \cdot [L]^a \cdot [L T^{-1}]^b \cdot [M L^{-3}]^c$$

Matching powers:

$$\text{Mass (M): } 0 = c \Rightarrow c = 0$$

$$\text{Length (L): } 0 = 2 + a + b \Rightarrow a = -1$$

$$\text{Time (T): } 0 = -1 - b \Rightarrow b = 1$$

So:

$$\Pi_2 = \frac{\nu}{d U_\infty}$$

Taking its inverse:

$$\Pi_2^{-1} = \frac{U_\infty d}{\nu} = Re$$

Conclusion

From the Buckingham Π theorem, we conclude:

$$\frac{D}{\rho U_\infty^2 d^2} = f \left(\frac{U_\infty d}{\nu} \right) \Rightarrow C_D = f(Re)$$

This confirms that the flow characteristics, including drag, depend solely on the Reynolds number.

3.2 Simulations.

It is notable to say that in these simulations, the steady regime encompasses values of $1 < Re < 80$, transient flow is found at $80 < Re < 200$ and turbulent flow is found at $Re > 200$. Let us go over these cases one by one.

We have used different values of the Reynolds number in order to have a better picture of how changing this value affects the flow properties. Using $Re = \frac{\rho UD}{\mu}$:

Re	U_∞
0.1	0.00014607
1	0.0014607
4	0.005843
10	0.014607
20	0.02921
30	0.04382
45	0.06573
70	0.10226
80	0.11686
100	0.14607
120	0.17528
150	0.2191
170	0.24832
200	0.20214
250	0.36518
300	0.4382
10^3	1.46073

Table 1: U_∞ for different values of Re .

As it can be seen, for $Re < 1$, the velocity at the inlet becomes very close to 0 and thus, can be considered negligible. $Re = 1$ should not be chosen, as it is still very close to 0. It is from $Re > 4$ when two steady vortices start appearing, which can be seen at $Re = 10$. These vortices keep growing at $Re = 20$ until $Re > 40$, where they disappear. That is the reason why at $Re = 70$ they are not there.

At $Re = 80$, we start finding transient flow, where the von karman vortex street takes place. This vortex street keeps growing periodically for $Re = 100$, $Re = 120$, $Re = 150$ and $Re = 170$, until it loses its periodicity when it reaches $Re = 200$.

At $Re = 200$, the flow begins being turbulent. Here we find the boundary layer, which confines viscous effects. At $Re = 10^5$, the velocity is so high that the boundary layer is highly detached from the surface. Along this lab, we will study all of this accompanied by visual demonstrations.

Keep in mind that it is not a good idea to choose the transition values of the Reynolds number. These values are 1, 4, 80 and 200. This is because, as it will be shown in the graphs, the transition to go from the previous stage to the following one is taking place just at that value, so no notorious changes will be seen.

3.3 Streamlines and the vorticity contours.

3.3.1 For a low Reynolds number (STEADY):

Here, for $Re < 4$, the flow is steady, symmetric, and laminar, so we find a Stokes flow. Therefore, no separation or vortex shedding occurs and thus, the streamlines, which are perfectly symmetric, smoothly wrap around the cylinder, with no wake formation behind the cylinder. However, for $4 < Re < 40$, we find two steady vortices at the back of the cylinder. At $40 < Re < 80$, the vortices keep growing until they become unstable and turn to transient flow. About the velocity contours, it can be seen that the flow smoothly accelerates around the cylinder and slows down symmetrically behind it and the velocity gradient is highest near the cylinder surface.

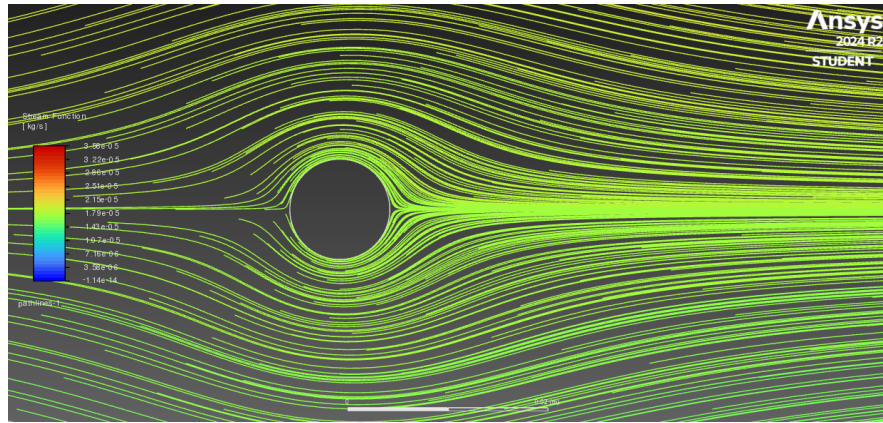


Figure 1: Streamlines and the vorticity contours for $Re = 0.1$

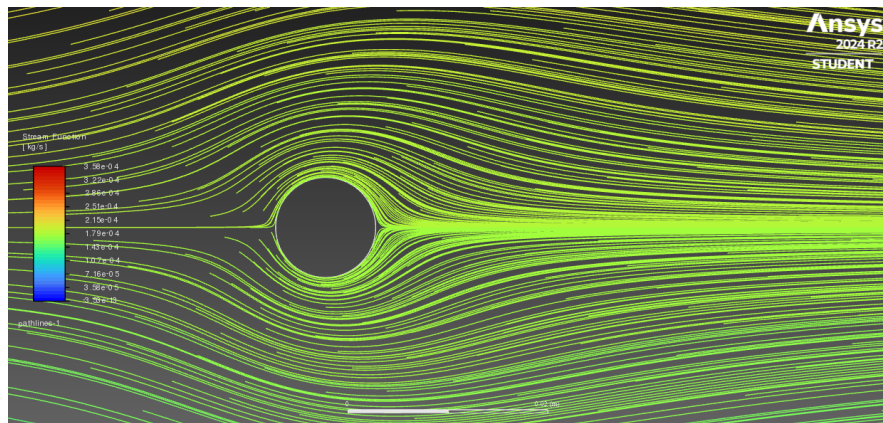


Figure 2: Streamlines and the vorticity contours for $Re = 1$

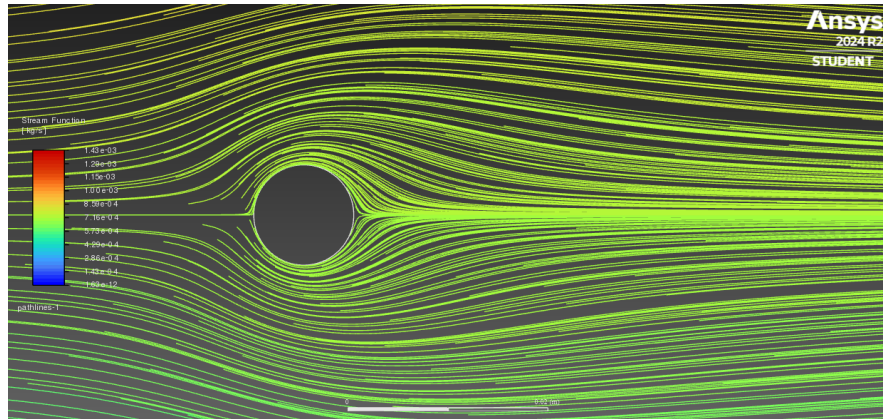


Figure 3: Streamlines and the vorticity contours for $Re = 4$

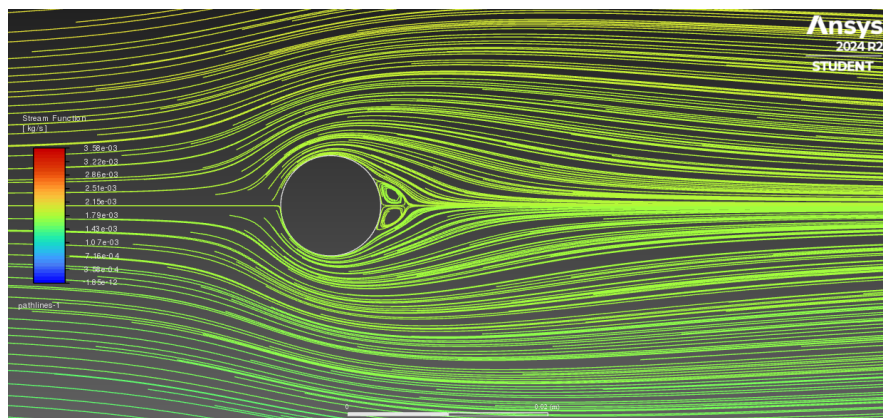


Figure 4: Streamlines and the vorticity contours for $Re = 10$

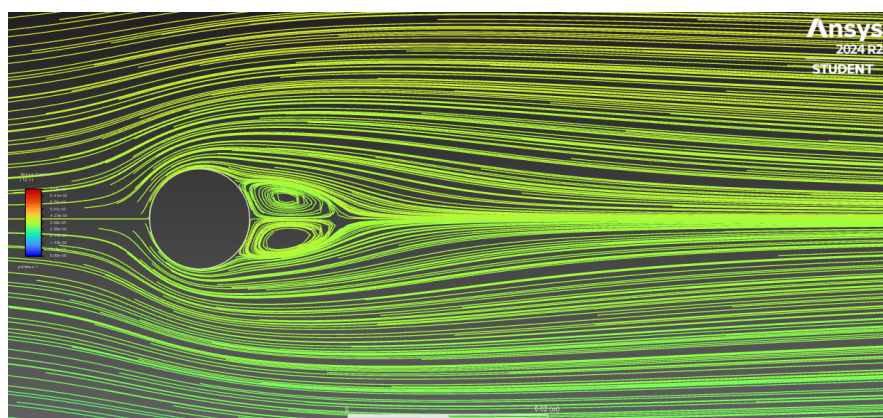


Figure 5: Streamlines and the vorticity contours for $Re = 20$

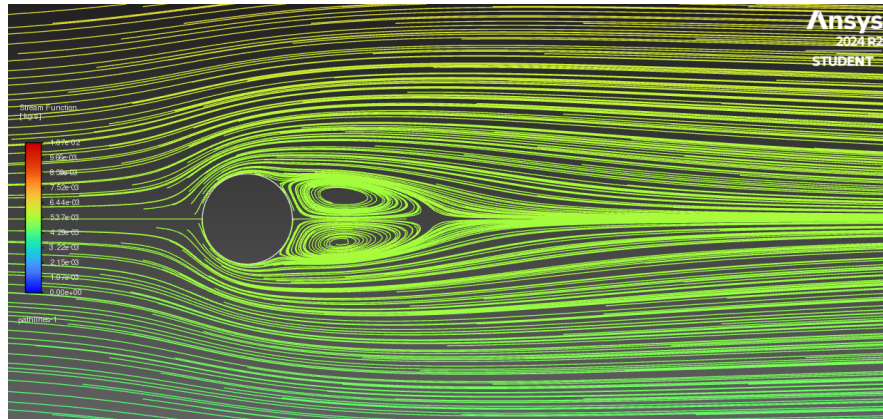


Figure 6: Streamlines and the vorticity contours for $Re = 30$

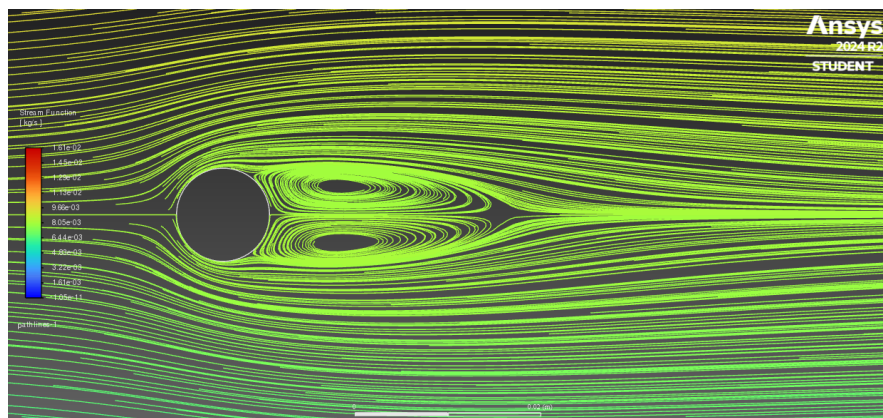


Figure 7: Streamlines and the vorticity contours for $Re = 45$

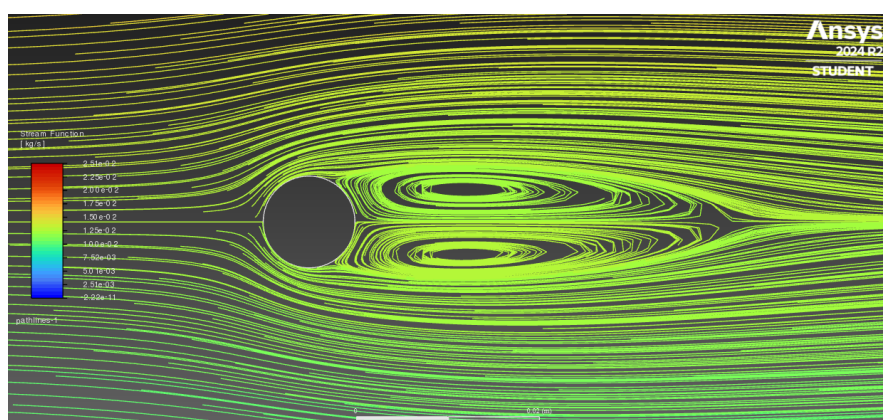


Figure 8: Streamlines and the vorticity contours for $Re = 70$

3.3.2 For a moderate Reynolds number (TRANSIENT):

As Re increases (for $Re > 80$), vortices appear due to alternating low and high velocity regions that develop downstream and become periodic. This is known as the von Kármán vortex street. About velocity, it is highest near the cylinder sides and decreases in the wake.

3.3.3 For a high Reynolds number (TURBULENT):

Here we find a fully developed turbulence, where the vortex shedding becomes irregular and chaotic, due to the fact that the wake grows and transitions to turbulence for $Re > 200$. This causes the boundary layer separation to occur earlier on the cylinder surface. The streamlines are highly distorted, showing unsteady vortex shedding. There are large velocity fluctuations in the wake and the separation point moves forward as Re increases.

3.4 Pressure Distribution for different values of the Reynolds Number.

3.4.1 For a low Reynolds number (STEADY):

Here, the flow remains attached to the surface without separation. As it can be noticed in the images, for really low values of Re , the pressure distribution is bisymmetrical, but as Re increases, the maximum pressure tends to be at the front of the cylinder and decreases as the flow reaches the bottom. For $45 < Re < 70$, there is a region of low pressure right behind the cylinder. Moreover, no suction peak at the top and bottom of the cylinder will take place.

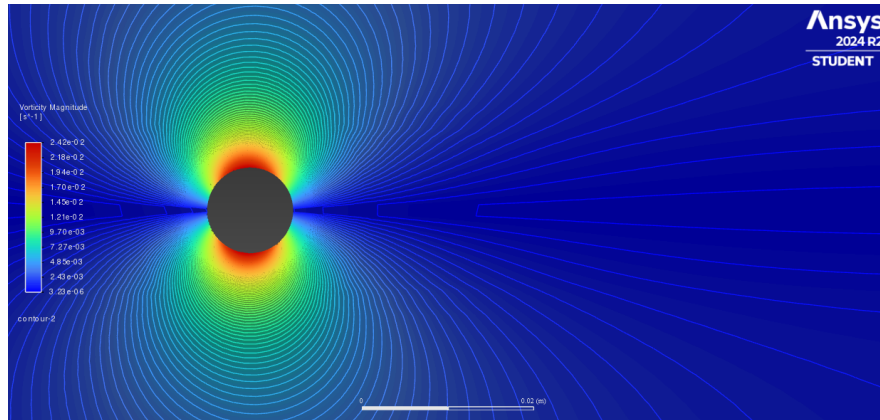


Figure 9: Pressure Distribution for $Re = 0.1$

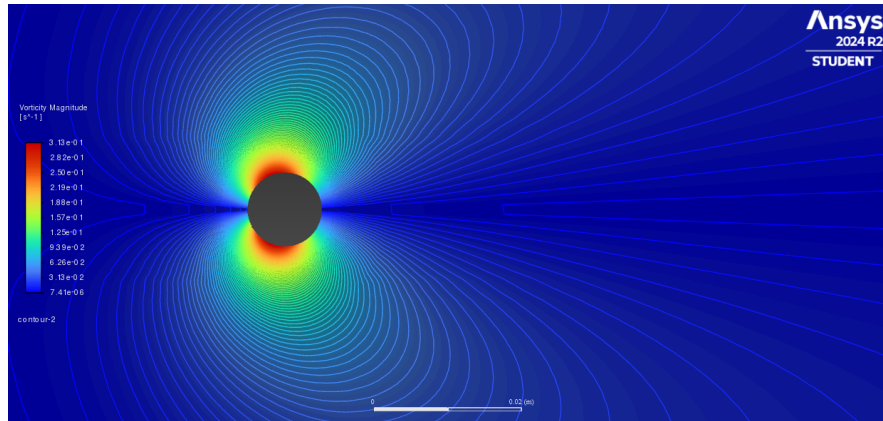


Figure 10: Pressure Distribution for $Re = 1$

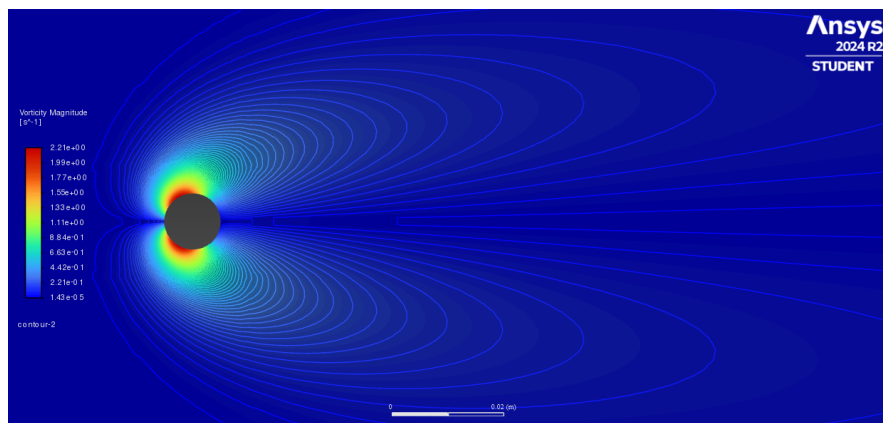


Figure 11: Pressure Distribution for $Re = 4$

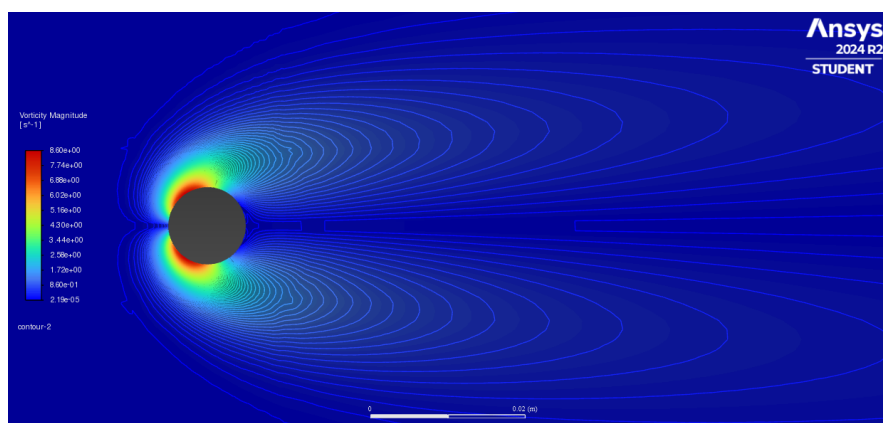


Figure 12: Pressure Distribution for $Re = 10$

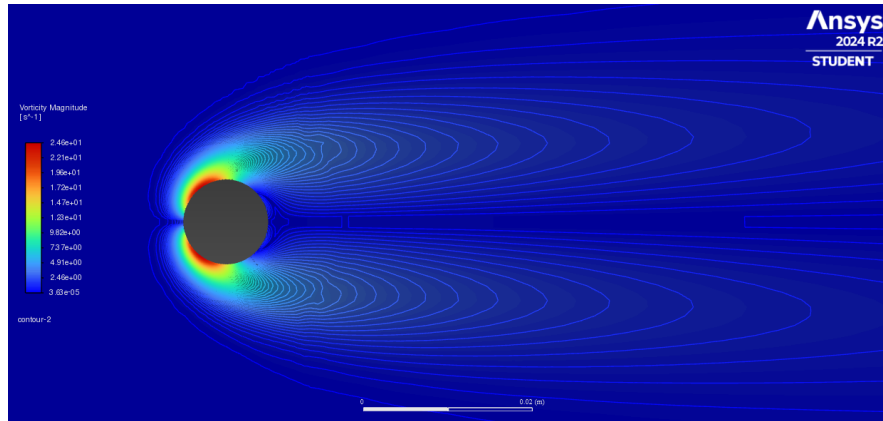


Figure 13: Pressure Distribution for $Re = 20$

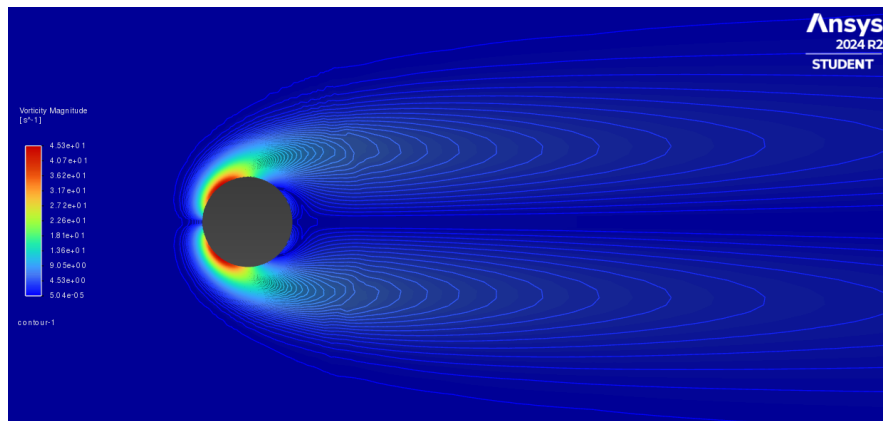


Figure 14: Pressure Distribution for $Re = 30$

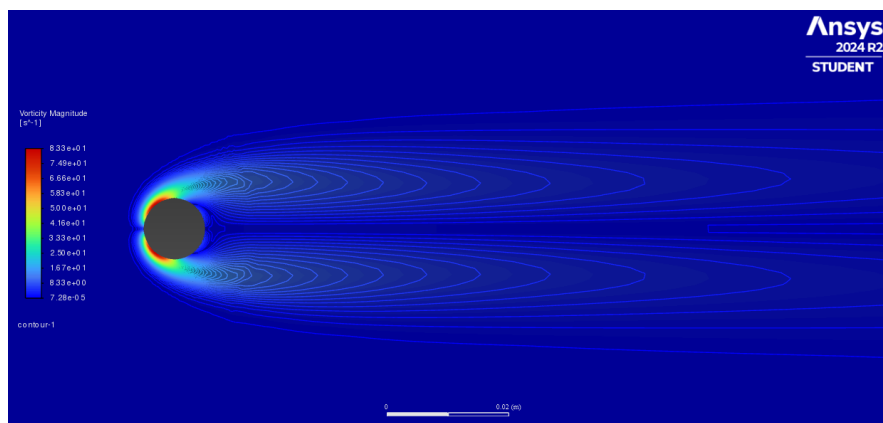


Figure 15: Pressure Distribution for $Re = 45$

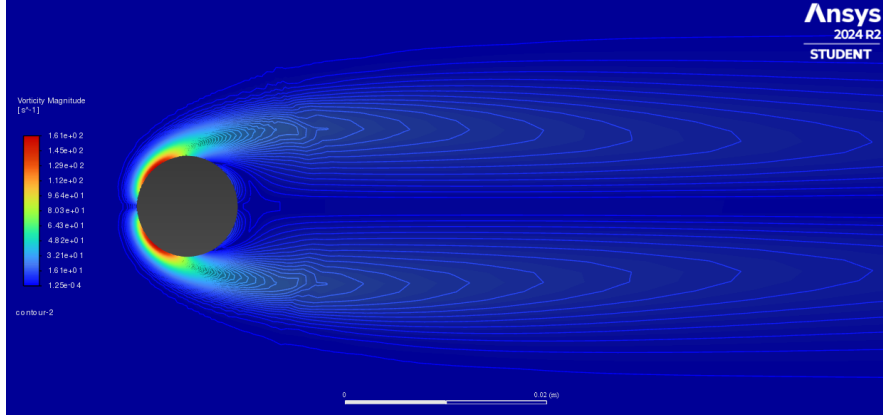


Figure 16: Pressure Distribution for $Re = 70$

3.4.2 For a moderate Reynolds number (TRANSIENT):

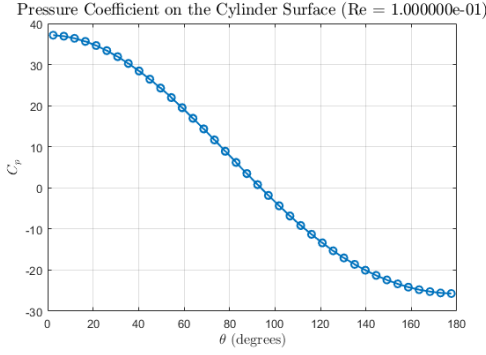
Here, flow separation starts at the rear, forming a small wake, which makes pressure to drop more steeply on the front side. We find a high c_p at the stagnation point $\theta = 0$. Suction peak appears near $\theta = 90$ due to acceleration around the cylinder and a sudden pressure recovery occurs in the wake region, around $\theta \approx 120$. Also, pressure is lower than inviscid predictions due to boundary layer effects.

3.4.3 For a high Reynolds number (TURBULENT):

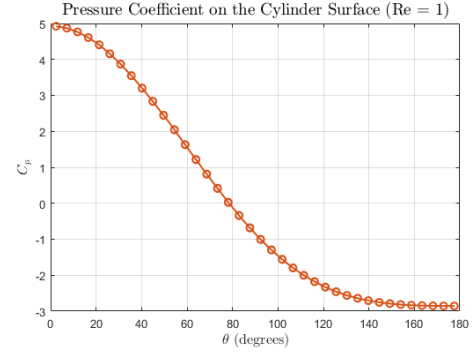
Here, as the flow separates earlier on the surface, a large wake region at the rear will lead to low pressure, leading to a high difference between front and rear pressure, making drag to increase significantly. Suction peak becomes more pronounced due to strong acceleration at the front and pressure remains low in the wake without recovery at $\theta = 180$.

3.5 Pressure coefficient on the cylinder surface as a function of the cylinder angle θ . (STEADY)

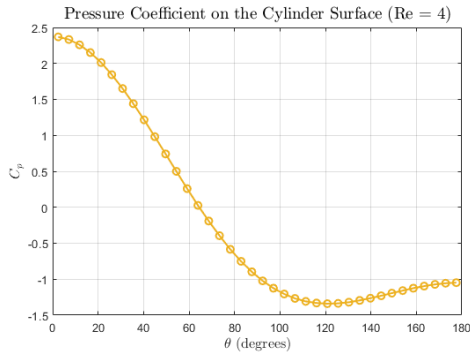
Let us evaluate the effect of changing the angle on the pressure coefficient. First, here are the graphs for the different cases:



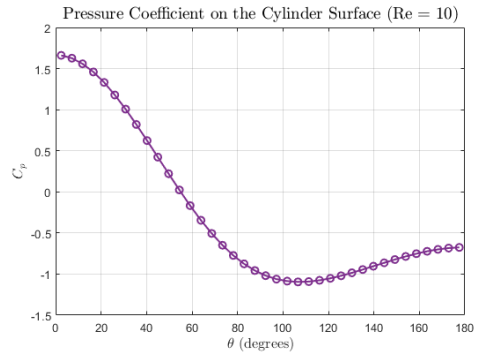
(a) Pressure Coefficient for $Re = 0.1$



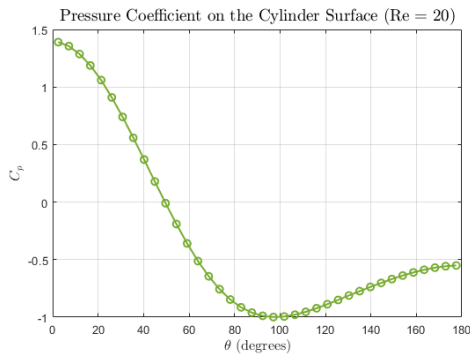
(b) Pressure Coefficient for $Re = 1$



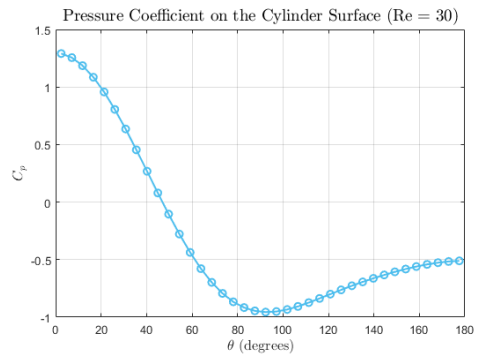
(c) Pressure Coefficient for $Re = 4$



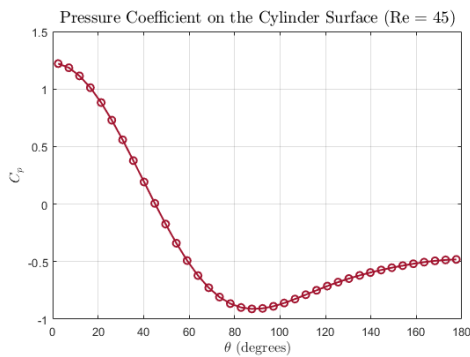
(d) Pressure Coefficient for $Re = 10$



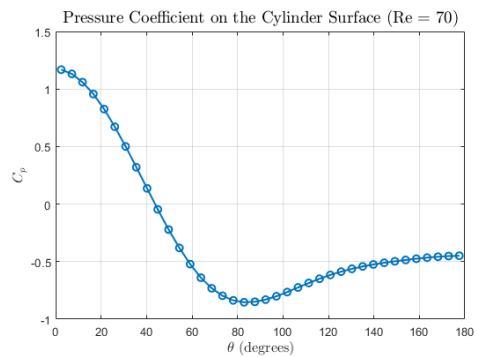
(e) Pressure Coefficient for $Re = 20$



(f) Pressure Coefficient for $Re = 30$



(g) Pressure Coefficient for $Re = 45$



(h) Pressure Coefficient for $Re = 70$

Figure 17: Pressure coefficient distributions for various Reynolds numbers

Now, here is a graph with all of the previous graphs merged, where we can compare the results:

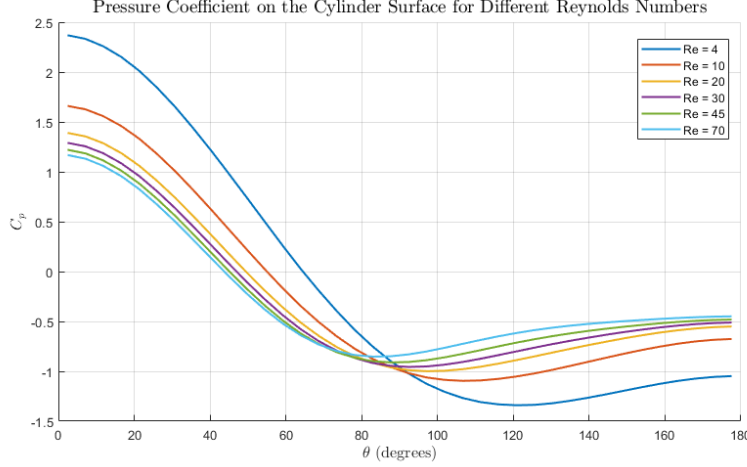


Figure 18: Pressure Coefficient for different values of Re

From this graph, it can be seen that the pressure coefficient is minimum for any Re number at around $80 < \theta < 120$. The smaller the Reynolds number, the higher the pressure coefficient for small values of θ but also the smaller for high values of θ . This is because, near the front of the cylinder (for small values of theta), the flow decelerates, which increases pressure and thus the pressure coefficient (according to the formula $c_p = \frac{p-p_\infty}{\frac{1}{2}\rho U^2}$). Towards the side or back (for higher angles), the viscous effect dominates, which does not allow sharp velocity to increase, which leads to less pressure drop and thus lower pressure gradients. Therefore, lower c_p .

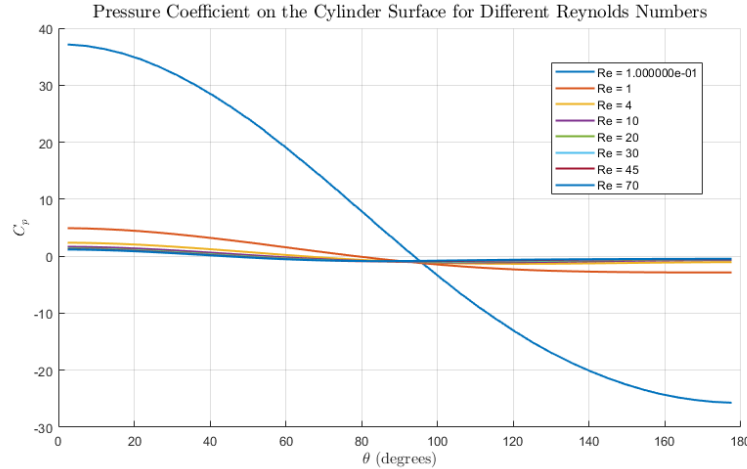


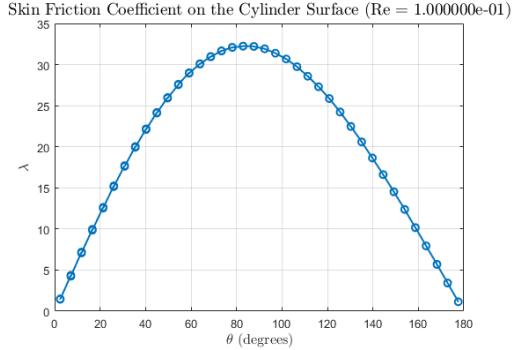
Figure 19: Pressure Coefficient for different values of Re

This graph demonstrates the aforementioned in a more visual and exaggerated way by using a $Re \ll 1$.

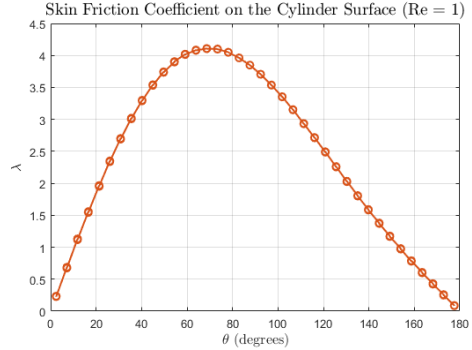
3.6 Friction coefficient on the cylinder surface as a function of the cylinder angle θ .

3.6.1 For a low Reynolds number (STEADY):

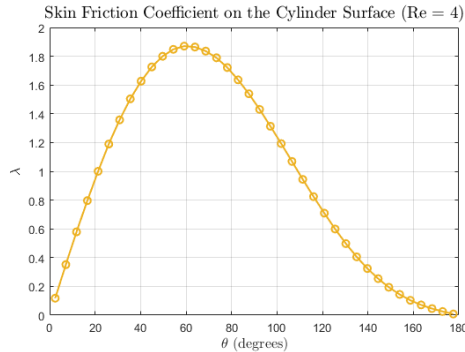
Note that, in this section, the angles just go from 0 to 180 because we find ourselves in the steady state, which is symmetric. Let us evaluate the friction coefficient for the steady case. Here are the separate graphs for each Reynolds number just so the reader can visualize the differences:



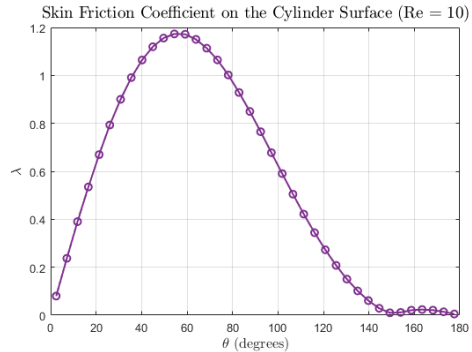
(a) Friction Coefficient for $Re = 0.1$



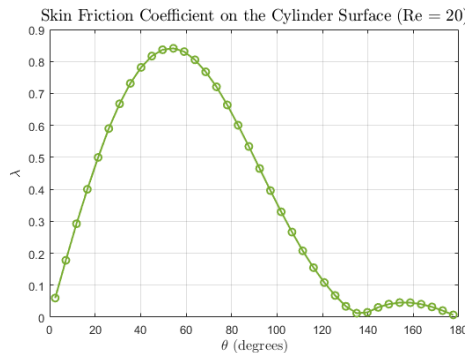
(b) Friction Coefficient for $Re = 1$



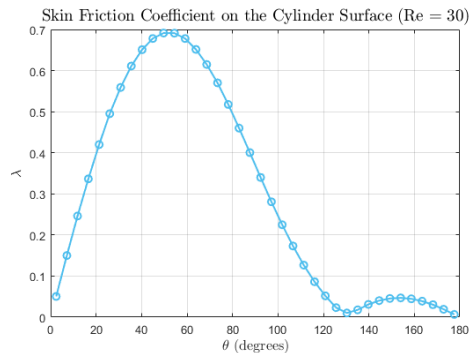
(c) Friction Coefficient for $Re = 4$



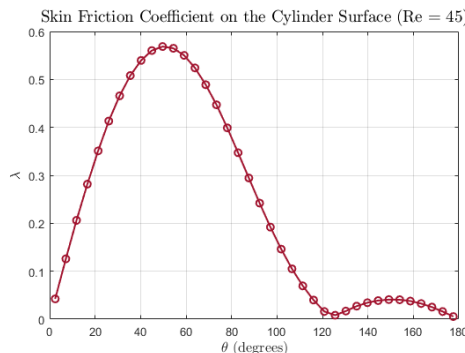
(d) Friction Coefficient for $Re = 10$



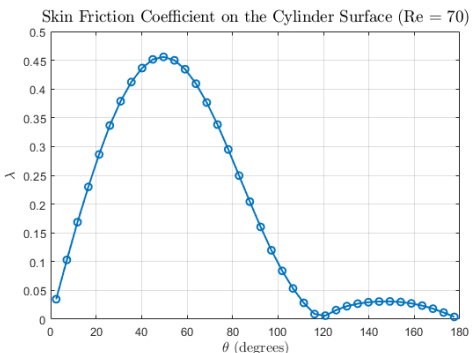
(e) Friction Coefficient for $Re = 20$



(f) Friction Coefficient for $Re = 30$



(g) Friction Coefficient for $Re = 45$



(h) Friction Coefficient for $Re = 70$

Figure 20: Friction coefficient distributions at various Reynolds numbers.

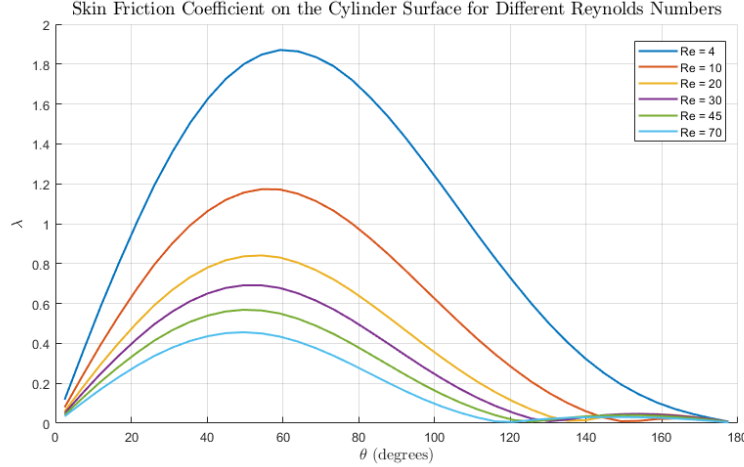


Figure 21: Friction Coefficient as a function of θ for different values of Re

From this last graph, by merging all of the graphs above, it can be seen that the maximum friction for any value of the Reynolds number is around $50 < \theta < 60$. It can also be noticed that the lower the Re, the higher the friction coefficient. In this case, $Re = 4$ is the one with the most friction. This is due to the fact that, according to $Re = \frac{\rho U D}{\mu}$, the higher the viscosity, the lower the Reynolds number. In this case, we find a Stokes flow where the viscosity dominates and the inertial effects are negligible. Due to the fact that viscosity is dominant, every bit of movement is opposed by it without the aid of inertia to carry the flow along. Therefore, the friction increases.

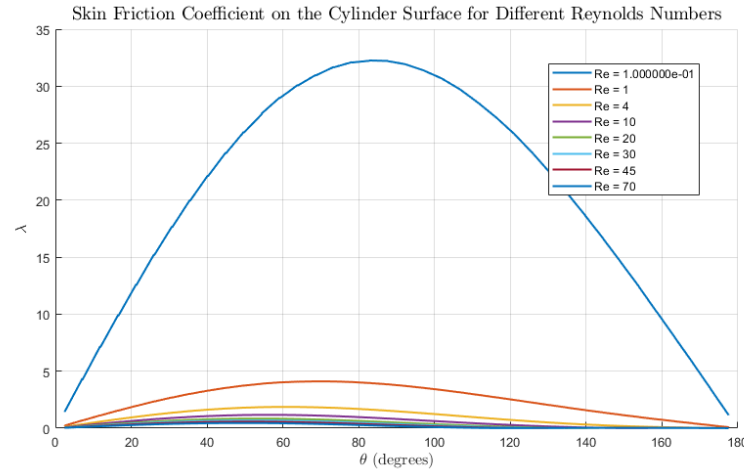


Figure 22: Friction Coefficient as a function of θ for different values of Re

Here it can be seen that for $Re \ll 1$, the friction coefficient increases a lot compared to the values used, again, demonstrating in a more visual way the effect that high viscosity makes in friction.

3.6.2 For a moderate Reynolds number (TRANSIENT):

Here, flow separation starts in the rear, at $\theta > 100$, making drag to decrease as the boundary layer grows along the surface. However, after separation, friction coefficient drops to zero because there is no wall contact. Again, friction coefficient is highest near the stagnation point.

3.6.3 For a high Reynolds number (TURBULENT):

Here, a turbulent boundary layer forms before separation, which happens earlier than in moderate Re cases, making friction to remain high longer due to the fact that turbulence is delaying separation. Now, the friction coefficient has its higher peak at the front due to stronger acceleration, it suffers a rapid decrease as the turbulent boundary layer thickens and is finally followed by an abrupt drop to zero at the separation point.

3.7 Separation point as a function of the Reynolds number.

3.7.1 For a low Reynolds number (STEADY):

For a low Reynold's number, viscous forces dominate. Thus, the flow shows a horizontal symmetry due to negligible inertial effects. At values of $Re < 10$, in our case, no separation at all occurs. It is at $Re = 10$ when there is a huge initial separation angle of 150° that decreases continuously as the Re increases.

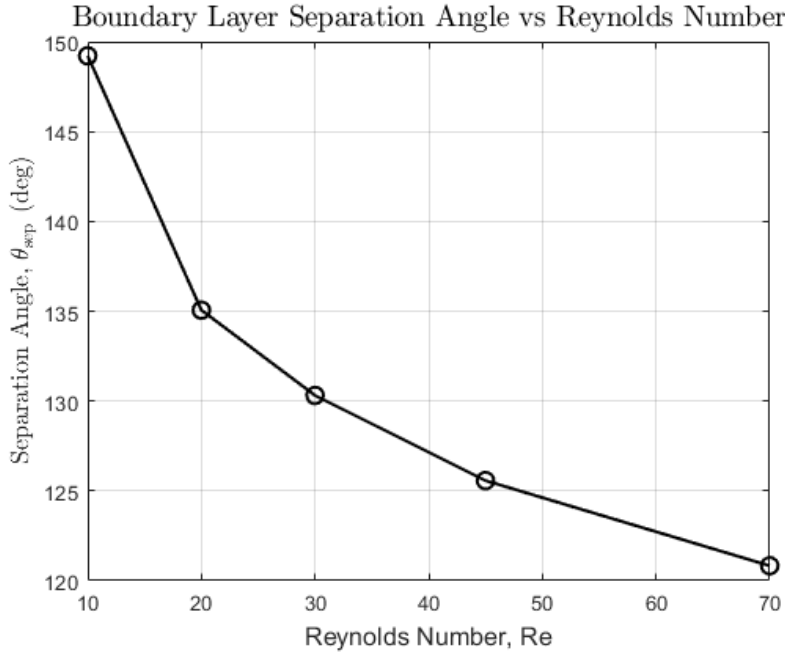


Figure 23: Boundary Layer Separation

3.7.2 For a moderate Reynolds number (TRANSIENT):

Inertial forces grow with Reynold's Number, creating an increasing instability in the wake of the cylinder. For $Re > 80$ the flow changes into a Von Kármán vortex, patterns characterised with periodic vortex shedding. As Re grows bigger and bigger the separation point moves upstream, so for a $Re \approx 100 - 200$ the angles $\theta \approx 80 - 100$. The wake widens, creating a much higher drag due to a larger low-pressure region.

3.7.3 For a high Reynolds number (TURBULENT):

For $Re > 200$ the wake becomes fully turbulent, but the boundary layer, however, remains laminar until $Re > 3 \times 10^5$. Vortex shedding persists but loses regularity, and the separation point remains fixed at $\theta \approx 80 - 100$. At very large values $Re > 3 \times 10^5$, the boundary layer becomes turbulent, and the separation point recedes to $\theta \approx 120 - 140$.

3.8 Oscillation frequency (f) and the Strouhal number, as a function of the Reynolds number.

3.8.1 For a low Reynolds number (STEADY):

At very low Re , viscous forces dominate, resulting in a steady, symmetric flow. The boundary layer remains attached due to strong viscous damping, and vorticity diffuses uniformly. The oscillation frequency is close to 0, as there are no inertial instabilities to drive oscillations. Since there's no dominant frequency $St = 0$.

3.8.2 For a moderate Reynolds number (TRANSIENT):

For moderate Re values periodic vortex shedding begins to appear at the value of $Re \approx 80$. By the time $Re > 100$ these vortexes are fully periodic. The oscillation frequency increases approximately linearly with Re until it reaches a maximum value of 8 Hz at $Re = 300$. This means that higher flow rate or fluid velocity leads to faster oscillations. Whereas for the Strouhal number, it can be seen that it rises initially, then reaches its maximum value at $Re \approx 170$ and $St \approx 0.2$ and ends up flattening out, suggesting that the nature of the flow oscillation becomes more consistent at higher Reynolds numbers.

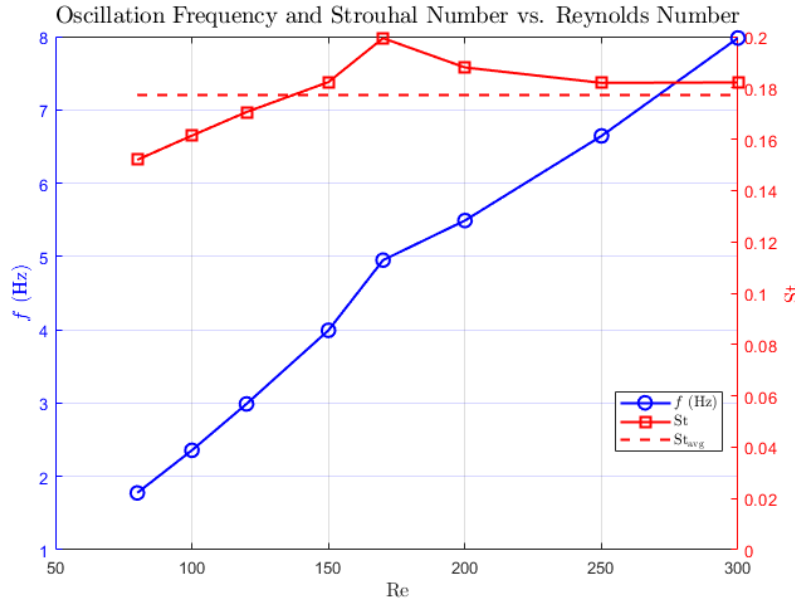


Figure 24: Friction Coefficient for Transient Flow.

3.8.3 For a high Reynolds number (TURBULENT):

For $Re < 300$, the flow is transient and acts just like the previous graph. However, when the flow enters the turbulent regime, according to the graph, around $Re = 300$, the frequency starts to decay very sharply, as well as the Strouhal number, which does it in a continuous way. This suggests a breakdown of the coherent periodic structures that were present in the transient flow.

This is one of the main characteristics of turbulent flow, as in this regime, the vortex shedding becomes irregular or chaotic, making oscillations to become less dominant and harder to characterize with a single frequency.

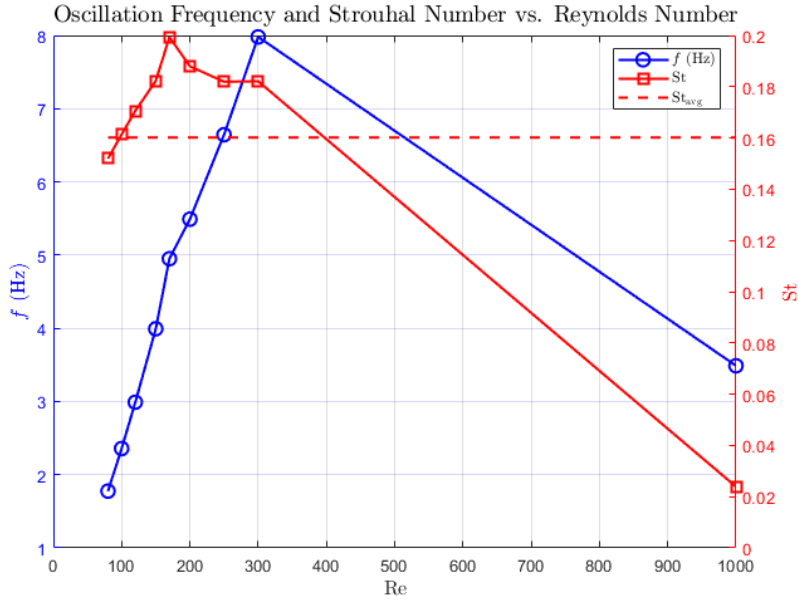


Figure 25: Friction Coefficient for Turbulent Flow.

3.8.4 Analysis of the Fast Fourier Transform and Strouhal number maintenance

We used the Fast Fourier Transform (FFT) in order to determine the frequency of the flow over a cylinder, allowing us to find the Strouhal number ($St = \frac{f \cdot d}{U_\infty}$) as a function of the Reynolds number (Re). We used the FFT algorithm to transform the velocity data obtained with ANSYS FLUENT into the frequency domain, the function identifies the main vortex shedding frequency by locating the highest peak in the positive frequency spectrum after removing the unsteady part, finally it removes the average trend from the proportioned data.

The Strouhal number remains relatively constant at 0.2 when $Re = 80$ to 300 because the shedding frequency scales linearly with the free stream velocity, this is a result of the shape of the cylinder and the steady flow conditions in the range before the flow becomes fully turbulent, where the scaling factor $k \approx 0.2$ remains valid until the boundary layer becomes turbulent at $Re \approx 3 \times 10^5$.

3.9 Animation of the vorticity contours using CFD Post

3.9.1 For a low Reynolds number (STEADY):

For low Reynolds number values steady symmetric contours appear behind the cylinder. As this value of Re is low, there is not any shedding, so there is almost no vorticity in the wake. Therefore, only two weak stationary recirculation bubbles appear at the sides of the cylinders. Thus, it would not make sense to do an animation for this case.

3.9.2 For a moderate Reynolds number (TRANSIENT):

As Reynolds number gets higher and higher, inertia forces get more intense and thus, some periodic vortex shedding appear, in the form of Von Kármán vortexes. These maintain a clear Strouhal rhythm. And at the separation points of the flow very high vorticity contours appear.

3.9.3 For a high Reynolds number (TURBULENT):

Once Re is high enough, the previous symmetric steady wake turns into a chaotic turbulent one. Vorticity in the flow also increases drastically, disrupting the periodicity of the wake. The turbulence creates a lot of vorticity without a clear structure.

4 Discussion of Results

4.1 b) Application of the Π Theorem

Dimensional analysis indicates that the flow past a circular cylinder depends solely on the Reynolds number, $Re = U_\infty d/\nu$, where U_∞ is the freestream velocity, d is the cylinder diameter, and $\nu = \mu/\rho$ is the kinematic viscosity. To verify this, we conduct numerical simulations using ANSYS Fluent, comparing two configurations at identical Re . The first uses default air properties (e.g., $\rho = 1.225 \text{ kg/m}^3$, $\mu = 1.81 \times 10^{-5} \text{ Pa}\cdot\text{s}$) with a cylinder diameter of $d = 1 \text{ cm}$, while the second employs dimensionless properties and geometry, setting $\rho = \mu = d = 1$, with U_∞ adjusted to match the same Re .

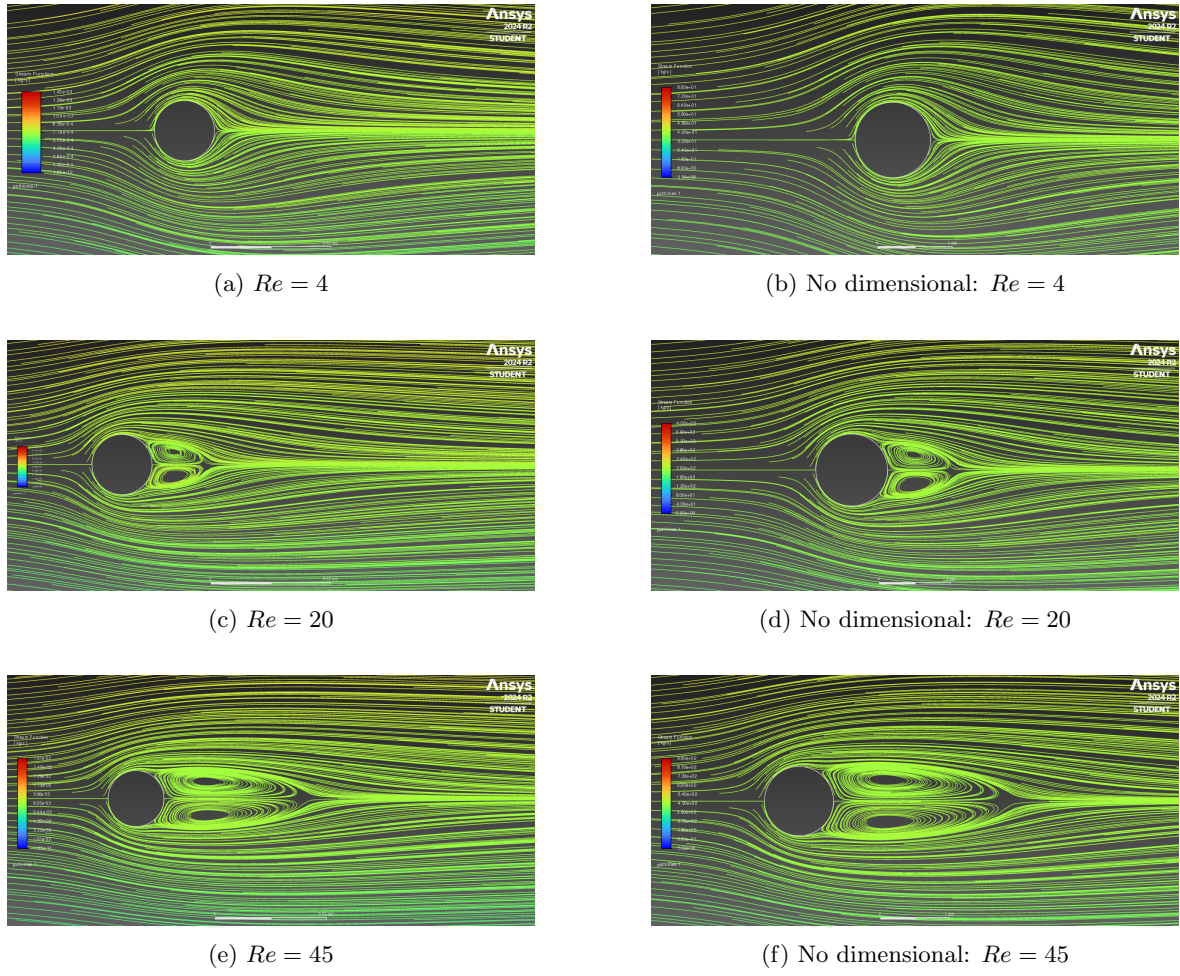


Figure 26: Non dimensional comparison of the streamlines.

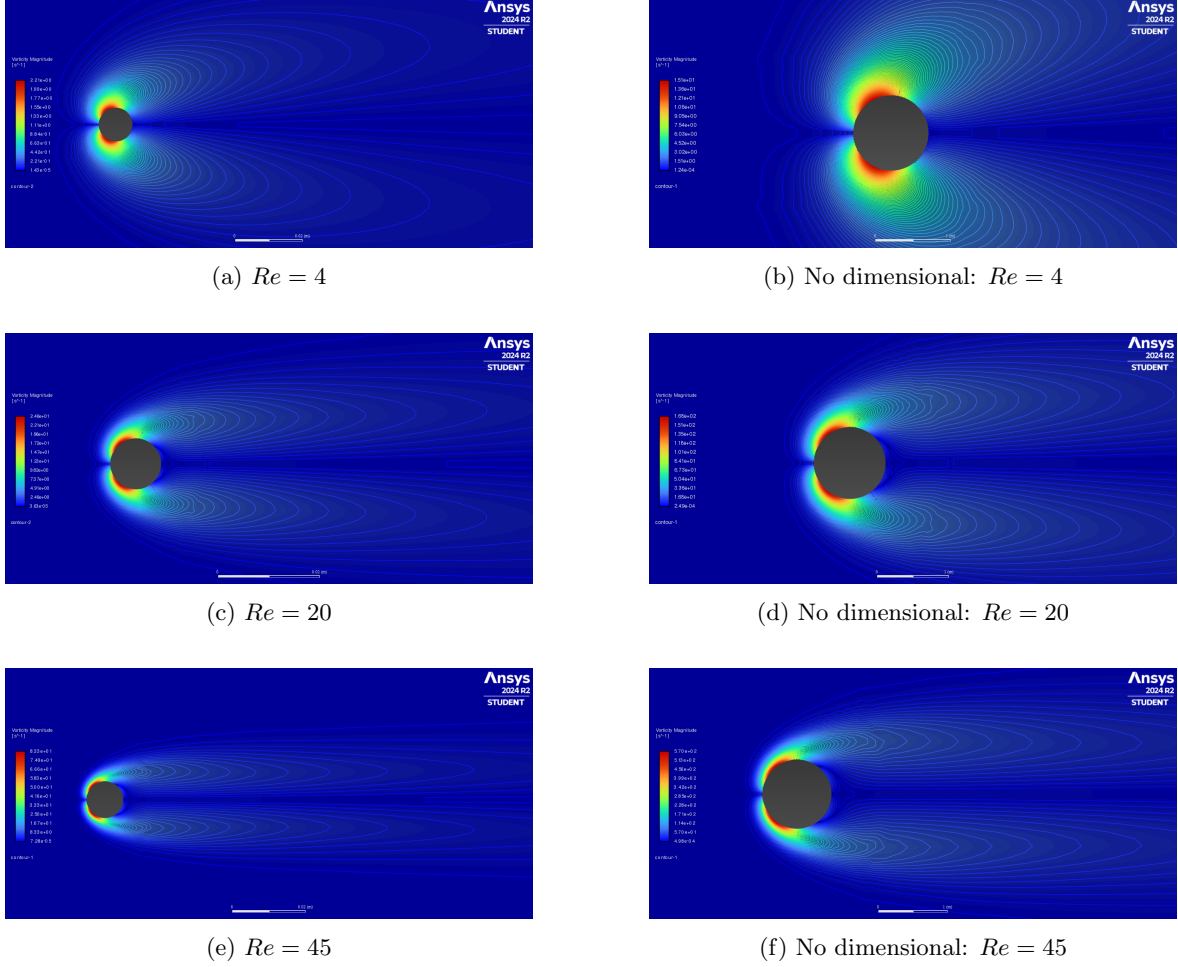


Figure 27: Non dimensional comparison of the vorticity magnitudes.

This comparison tests the principle of dynamic similarity, ensuring that flow characteristics—such as pressure distributions and flow patterns—remain consistent across these setups, validating the theoretical dependence on Re alone.

4.2 Default vs non-dimensional air properties

Quantitatively, they are going to be different but qualitatively, the default properties are going to match the non-dimensional ones. As we can see, since the Reynolds number is identical, the pressure variation around the cylinder, the velocity field and the C_d is the same when made dimensionless. However, due to differences in numerical scaling, the force values (in Newtons) will be different, but their non-dimensionalized form will match. The flow separation point should remain unchanged since it primarily depends on the Reynolds number.

4.3 Conclusion on Vorticity Contour Animations

In this study, the original intent was to create animations of vorticity contours for all cases using CFD Post, as recommended, and save them in AVI format. However, due to corrupted ANSYS files, CFD Post could not be utilized. As an alternative, we employed the Solution Animations tool within ANSYS Fluent's Calculation Activities module. For each case, we configured the simulation to capture vorticity contours—equivalent to the velocity curl as required—at every timestep of 0.02 seconds. These contours were saved as individual images, effectively providing a frame-by-frame representation of the vorticity evolution. While this approach deviates from the suggested AVI format, it achieves the same objective of visualizing the dynamic behavior of vorticity across the simulated flow regimes, ensuring the analysis remains comprehensive despite the technical limitations encountered.

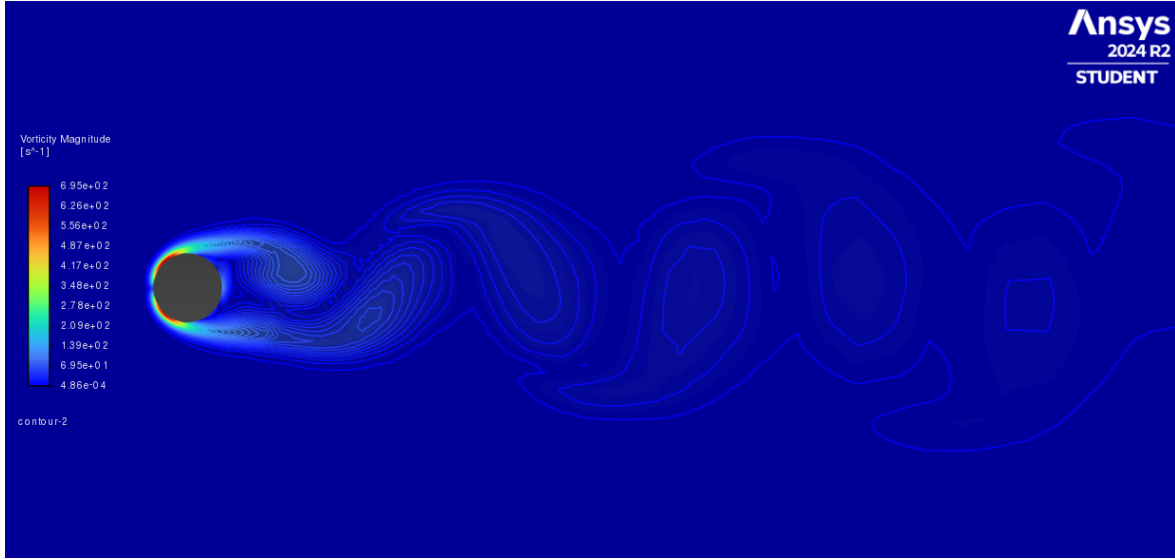


Figure 28: Example of the Von-Karman Vortex for $Re = 170$

5 Comments and conclusions.

This lab experiment successfully demonstrated how varying Reynolds numbers influence flow behavior around a circular cylinder. At low Reynolds numbers, the flow remained symmetric with small separation bubbles. At moderate Reynolds numbers, periodic vortex shedding was observed, forming a von Kármán vortex street. At high Reynolds numbers, the boundary layer transitioned to turbulence, leading to reduced drag due to delayed flow separation. The numerical simulations in ANSYS Fluent provided insights into the pressure distribution, friction coefficients, and oscillation frequencies, reinforcing key concepts in fluid mechanics. Future extensions of this study could involve exploring different turbulence models or analyzing three-dimensional effects to enhance the accuracy of results.

All in all, this laboratory practice showed us how ANSYS Fluent is used to compute the flow around a given cylinder. As we have stated by applying Vaschy-Buckingham-Pi Theorem and later demonstrated with the use of ANSYS, the properties of the flow around the cylinder are just dependent on Reynold's number. Furthermore, modifying that quantity gives a series of different, yet predictable, results that range from von Karman vortices to turbulent wakes.